$\mathcal{P},\mathcal{T}$-odd effects in YbCu, YbAg and YbAu

Johan David Polet,[1] Yuly Chamorro,[1,2] Lukáš F. Pašteka,[1,2,3] Steven Hoekstra,[1,2] Michał Tomza,[4] Anastasia Borschevsky,[1,2] and I. Agustín Aucar[1,2,5,a)]

[1)] *Van Swinderen Institute for Particle Physics and Gravity, University of Groningen, Nijenborgh 4, 9747 AG Groningen, The Netherlands*

[2)] *Nikhef, National Institute for Subatomic Physics, Amsterdam, The Netherlands*

[3)] *Department of Physical and Theoretical Chemistry, Faculty of Natural Sciences, Comenius University, Mlynská dolina, 84215 Bratislava, Slovakia*

[4)] *Faculty of Physics, University of Warsaw, Pasteura 5, 02-093 Warsaw, Poland*

[5)] *Instituto de Modelado e Innovación Tecnológica (UNNE-CONICET), Facultad de Ciencias Exactas y Naturales y Agrimensura, Universidad Nacional del Nordeste, Av. Libertad 5460, Corrientes, Argentina*

(Dated: 29 November 2024)

In this work, the molecular enhancement factors of the $\mathcal{P},\mathcal{T}$-odd interactions involving the electron electric dipole moment (W_d) and the scalar-pseudoscalar nucleon-electron couplings (W_s) are computed for the ground state of the bimetallic molecules YbCu, YbAg and YbAu. These systems offer a promising avenue for creating cold molecules by associating laser-cooled atoms. The relativistic coupled-cluster approach is used in the calculations and a thorough uncertainty analysis is performed to give accurate and reliable uncertainties to the obtained values. Furthermore, an in-depth investigation of the different electronic structure effects that determine the magnitude of the calculated enhancement factors is carried out, and two different schemes for computing W_d are compared. The final values for the enhancement factors are $(13.32 \pm 0.13) \times 10^{24}\ \frac{h\,\mathrm{Hz}}{e\,\mathrm{cm}}$, $(12.19 \pm 0.12) \times 10^{24}\ \frac{h\,\mathrm{Hz}}{e\,\mathrm{cm}}$ and $(2.36 \pm 0.48) \times 10^{24}\ \frac{h\,\mathrm{Hz}}{e\,\mathrm{cm}}$ for W_d, and $(-48.63 \pm 0.53)\ h\,\mathrm{kHz}$, $(-45.68 \pm 0.60)\ h\,\mathrm{kHz}$ and $(3.81 \pm 2.58)\ h\,\mathrm{kHz}$ for W_s, for YbCu, YbAg and YbAu, respectively.

I. INTRODUCTION

The current best description of elementary particles and their interactions is given by the Standard Model (SM) of particle physics[1]. This model is capable of describing almost all experimental observations (excluding gravitational interactions) and of accurately predicting a wide range of diverse phenomena, which is why over time it has been consolidated as a well-tested physical theory. However, it does not address some important observed effects, such as the matter-antimatter asymmetry in the universe, the neutrino oscillations, and the existence and nature of dark matter and dark energy[2,3]. Over the past decades, many new theories and extensions of the SM have been proposed to explain these phenomena[3,4]. Testing and restricting these theories is important for advancing our understanding of the fundamental laws of physics.

A promising way to test some of these theories is to search for effects due to the simultaneous non-conservation of spatial ($\mathcal{P}$) and time-reversal ($\mathcal{T}$) parities in atoms and molecules, such as those arising from the electric dipole moments (EDM) of electrons[5]. Interactions between these EDMs and electromagnetic fields violate both temporal and spatial invariance[6]. Within a $\mathcal{CPT}$-invariant theory ($\mathcal{C}$ refers to charge-conjugation symmetry), if $\mathcal{T}$ symmetry is violated, then the combined $\mathcal{CP}$ symmetry must also be non conserved, so that clearly $\mathcal{P},\mathcal{T}$ violation implies $\mathcal{CP}$ non conservation[2].

The sources of $\mathcal{CP}$ violation described by the SM lead to the prediction of a free-electron EDM d_e of approximately $5.8 \times 10^{-40}\,e\,\mathrm{cm}$[7]. However, more sources of $\mathcal{CP}$ violation beyond those predicted by the SM are needed to explain, for example, the observed matter-antimatter asymmetry. The additional sources of $\mathcal{CP}$ violation would in turn lead to an increase in the magnitude of the electron EDM (eEDM), even bringing it into the reach of present-day precision experiments[2]. Experimental searches for these phenomena are currently being carried out in atoms and molecules, taking advantage of the enhancement of the atomic and molecular EDMs. These arise from $\mathcal{P},\mathcal{T}$-violating interactions, mainly those taking place between the eEDMs and the large internal atomic or molecular electric fields, and also other $\mathcal{CP}$-odd nucleon-electron and nucleon-nucleon interactions[2,8–10]. Currently, the lowest upper limit of the eEDM is set at $|d_\mathrm{e}| < 2.1 \times 10^{-29}\,e\,\mathrm{cm}$. This upper limit was reported after measurements conducted by the National Institute of Science and Technology (NIST) on the HfF^+ molecular ion[11], and combining these results with those obtained by the ACME Collaboration in their analysis of the ThO molecule[12]. It is important to stress that if $\mathcal{CP}$ violation is assumed to arise exclusively from d_e in the NIST experiment (i.e., if the scalar-pseudoscalar nucleon-electron couplings are neglected), then the upper limit would be $|d_\mathrm{e}| < 4.1 \times 10^{-30}\,e\,\mathrm{cm}$. This lowest upper limit has already put considerable constraints on some of the theories beyond the SM[13,14].

In the ground state of a molecule with zero nuclear

a)Author to whom correspondence should be addressed. Electronic mail: agustin.aucar@conicet.gov.ar

spins and a single unpaired electron, there are two main contributions to the energy arising from $\mathcal{P},\mathcal{T}$-violating interactions, that is the interactions between the EDMs of the electrons and the electromagnetic fields and from the $\mathcal{P},\mathcal{T}$-odd scalar-pseudoscalar nucleon-electron (S-PS-ne) neutral-current interactions[9,15]. Since the effects of the eEDM and the S-PS-ne interactions are enhanced by the molecular electronic structure, the two corresponding molecular enhancement factors W_d (related to d_e) and W_s (which enhances the S-PS-ne interactions) are of particular interest.

The choice of molecule for the measurements has a significant impact on the sensitivity of the experiment due to, among others, the system-dependent enhancement of the $\mathcal{P},\mathcal{T}$-odd effects. Since in open-shell molecules that contain only one heavy element this enhancement scales roughly as the cube of the atomic number of the heavier nucleus to which the unpaired electron is strongly linked to[10,16,17], some heavy-element-containing molecules have an advantage over other systems. Furthermore, practical experimental considerations play a crucial role in selecting a candidate for experiments. For example, the use of ultra-cold molecules increases interaction times and hence the experimental precision[18]. Therefore, the laser-coolability of the selected molecule provides a clear advantage. Various molecular properties relevant for precision measurements (e.g., laser coolability and sensitivity to the measured phenomena, but also many others) can be determined theoretically before experimental investigations in support of such experiments. In particular, the enhancement factors cannot be measured and must be provided based on accurate electronic structure calculations.

In this work, we investigate the sensitivity of the YbCu, YbAg, and YbAu molecules to $\mathcal{P},\mathcal{T}$-violating phenomena. These systems are of particular interest since they contain two metal atoms. Theoretically, this means that these atoms can be laser-cooled separately and then associated into a molecule afterward, eliminating the need to laser-cool the molecule as a whole[19–21]. So far, laser-cooling of Yb and Ag atoms has been demonstrated[22,23]. Laser-cooling of Cu and Au has not been demonstrated yet, but cooling schemes have been proposed[24]. Furthermore, these polar molecules have large molecular-frame electric dipole moments, due to the large electronegativity of the coinage-metal atoms, allowing for their easy polarization. In particular, YbAg is considered a promising candidate for a next-generation clock-transition eEDM measurement[21].

No experiments have been performed so far on YbCu, YbAg, or YbAu, but several experimental groups pursue the ultra-cold formation of other Ag-containing molecules[25–28]. However, high-accuracy calculations of the potential energy curves, molecular-frame electric dipole moments, electric quadrupole moments, and static electric dipole polarizabilities of the present systems were recently performed[29]. Here we employ the four-component (4c) relativistic coupled-cluster (CC) approach to calculate the enhancement factors of the $\mathcal{P},\mathcal{T}$-violating interactions between the eEDMs and the electric fields in the systems, W_d, and of the $\mathcal{P},\mathcal{T}$-odd S-PS-ne interactions, W_s. The enhancement factors are determined for the ground states, $X\,^2\Sigma^+_{\frac{1}{2}}$, of the three molecules. We also carry out an extensive computational study to assign uncertainties to the calculated values.

In open-shell molecules containing at least one non-zero nuclear spin I, some internal nuclear interactions lead to nuclear spin-dependent molecular $\mathcal{P},\mathcal{T}$-violating effects, such as magnetic interactions between the electrons and the nuclear magnetic quadrupole moment (NMQM), which appears for nuclear spin $I \geq 1$[30,31]. These effects are, however, outside the scope of this work.

Section II covers the main theoretical aspects of this work, detailing how both enhancement factors can be obtained from effective Hamiltonians. Section III contains a description of the methods employed to calculate these factors, as well as the scheme used for geometry optimization. Next, Section IV presents the obtained enhancement factors and their dependence on effects such as the choice of the nuclear charge density model, the method for treatment of electron correlation, the choice of the basis set, and the internuclear distances. Finally, Section V contains a concise summary of our findings.

II. THEORY

The $\mathcal{P},\mathcal{T}$-violating interactions involving the EDMs of atoms or molecules produce non-zero linear Stark shifts in the limit of vanishingly small applied electric fields. These interactions originate from many different sources, but mainly from the EDMs of electrons and nucleons, as well as from the $\mathcal{P},\mathcal{T}$-violating nucleon-nucleon current interactions and the $\mathcal{P},\mathcal{T}$-odd electron-quark interactions[32]. In particular, for open-shell linear molecules in $X\,^2\Sigma_{\frac{1}{2}}$ ground states, such as the systems treated in this paper, the interactions between eEDMs and electromagnetic fields and the $\mathcal{P},\mathcal{T}$-odd S-PS-ne neutral-current interactions dominate[33]. In these cases, the effective spin-rotation Hamiltonian that includes only nuclear-spin-independent $\mathcal{P},\mathcal{T}$-odd interactions (i.e., neglecting the interactions between electrons and NMQMs) can be written as[9,34]

$$\hat{H}_\mathrm{sr}^{\mathcal{P},\mathcal{T}-\mathrm{odd}} = \left(\sum_K W_{\mathrm{s},K}\, k_{\mathrm{s},K} + W_\mathrm{d}\, d_\mathrm{e}\right) \hat{\Omega}, \qquad (1)$$

where the $\mathcal{P},\mathcal{T}$-odd dimensionless operator $\hat{\Omega} = \hbar^{-1}\mathbf{J}_\mathrm{e}\cdot\mathbf{n}$ is the scalar projection of the reduced total electronic angular momentum operator $\mathbf{J}_\mathrm{e}/\hbar$ onto the unit vector $\mathbf{n}$. The direction and sense of this vector operator $\mathbf{n} = \boldsymbol{\mu}/|\boldsymbol{\mu}|$ are given by the electric dipole moment of the system in the molecular frame, $\boldsymbol{\mu}$. For a linear molecule, the direction of this unit vector is given by the internuclear axis, while its sense depends on the distribution of the nuclear and electronic charge densities in the reference frame attached to the molecule. Here, $\hbar = h/(2\pi)$ is the reduced Planck constant. The sum in Eq. (1) runs over all the nuclei K in the system. In systems where

one nucleus is significantly heavier than the other (and where the unpaired electron is mostly located on that heavy nucleus), this sum typically reduces to a single term. We also note that $k_{\mathrm{s},K}$ is specific to each nucleus K, i.e., it depends on both the proton and the neutron numbers. Both these points will become important later and are discussed in Section II B.

To compute the enhancement factors, the effects of the eEDM and the S-PS-ne interactions are taken as perturbations on the 4c relativistic Dirac–Coulomb (DC) Hamiltonian. Since d_{e} and $k_{\mathrm{s},K}$ are small quantities, the effects arising from both interactions are minute. Therefore, first-order perturbation treatment will already yield highly accurate results.

Within the Born-Oppenheimer approximation, the 4c DC (clamped-nuclei) Hamiltonian is given by

$$\hat{H}^{(0)} = \sum_i \left[c\boldsymbol{\alpha}_i \cdot \hat{\boldsymbol{p}}_i + \boldsymbol{\beta}_i m_e c^2 - \mathbb{1}_{4\times4} \sum_K e\Phi_K(\boldsymbol{r}_i) \right] - \mathbb{1}_{4\times4}\, \frac{1}{2} \sum_{i\neq j} e\Phi_j(\boldsymbol{r}_i) \;+\; \mathbb{1}_{4\times4}\, U^{\mathrm{nuc}}, \tag{2}$$

where

$$\Phi_K(\boldsymbol{r}_i) = \frac{1}{4\pi\varepsilon_0} \int \frac{\rho_K(\mathbf{r}')}{|\mathbf{r}_i - \mathbf{r}'|} d^3\boldsymbol{r}', \tag{3}$$

$$\Phi_j(\boldsymbol{r}_i) = -\frac{1}{4\pi\varepsilon_0} \frac{e}{|\boldsymbol{r}_i - \boldsymbol{r}_j|}, \tag{4}$$

$$U^{\mathrm{nuc}} = \frac{1}{8\pi\varepsilon_0} \sum_{K\neq L} \frac{Z_K Z_L e^2}{|\boldsymbol{R}_K - \boldsymbol{R}_L|}. \tag{5}$$

In Eqs. (2), (3), and (4), as well as in all this work, the SI system of units was used. Here, $\mathbb{1}_{4\times4}$ is the 4×4 identity matrix, the operator $\Phi_K(\boldsymbol{r}_i)$ refers to the Coulomb electric potential produced by the nucleus K at the position of the i-th electron, whereas $\Phi_j(\boldsymbol{r}_i)$ is the electric potential created by electron j at the position $\boldsymbol{r}_i$. The last term in Eq. (2) is the potential energy arising from all the nucleus-nucleus Coulomb interactions. According to Gauss' law, and considering that the root-mean-square radius of any nucleus is about five orders of magnitude smaller than the distance between the centers of any two nuclei in a molecule, the repulsive potential energy arising from the interaction between two given nuclei (provided that their electric charge distributions are described by spherically symmetric functions) can be safely approximated as the interaction between two point-type nuclei with their total charges concentrated in their centers. This approximation is standard in molecular physics. In addition, c is the speed of light in vacuum, m_e is the electron rest mass, e is the elementary charge, ε_0 is the vacuum permittivity, $\rho_K(\mathbf{r}')$ is the charge density distribution of nucleus K at an arbitrary position $\mathbf{r}'$, Z_K and Z_L are the atomic numbers of nucleus K and L, respectively, and $\boldsymbol{r}_i$, $\boldsymbol{r}_j$, $\boldsymbol{R}_K$ and $\boldsymbol{R}_L$ are the position vectors of the electrons i and j, and nuclei K and L, respectively. Here and in what follows, the sums over i and j run over all the electrons in the molecule, whereas the sums over K and L run over all the nuclei of the system. Besides, $\hat{\boldsymbol{p}}_i = -i\hbar\hat{\boldsymbol{\nabla}}_i$ is the linear momentum (vector) operator of electron i, while $\boldsymbol{\alpha}_i$ and $\boldsymbol{\beta}_i$ are the well-known 4×4 Dirac matrices in standard representation for the same electron. In this representation, they are expressed as

$$\boldsymbol{\alpha} = \begin{bmatrix} \boldsymbol{\emptyset}_{2\times2} & \boldsymbol{\sigma} \\ \boldsymbol{\sigma} & \boldsymbol{\emptyset}_{2\times2} \end{bmatrix}, \qquad \boldsymbol{\beta} = \begin{bmatrix} \mathbb{1}_{2\times2} & \boldsymbol{\emptyset}_{2\times2} \\ \boldsymbol{\emptyset}_{2\times2} & -\mathbb{1}_{2\times2} \end{bmatrix}. \tag{6}$$

Here, $\mathbb{1}_{2\times2}$ and $\boldsymbol{\emptyset}_{2\times2}$ are the 2×2 identity and null matrices, respectively, and

$$\boldsymbol{\sigma} = \begin{bmatrix} 0 & 1 \\ 1 & 0 \end{bmatrix} \hat{\mathbf{i}} + \begin{bmatrix} 0 & -i \\ i & 0 \end{bmatrix} \hat{\mathbf{j}} + \begin{bmatrix} 1 & 0 \\ 0 & -1 \end{bmatrix} \hat{\mathbf{k}} \tag{7}$$

is the vector of Pauli matrices, with $\hat{\mathbf{i}}$, $\hat{\mathbf{j}}$ and $\hat{\mathbf{k}}$ being the unit vectors in Cartesian coordinates, and $i = \sqrt{-1}$ being the imaginary unit.

A. eEDM enhancement factor W_{d}

The effects on hydrogenic atoms arising from a $\mathcal{P},\mathcal{T}$-odd interaction between the permanent EDM of a single electron, parallel to its spin, and an electromagnetic field have been studied for the first time by Salpeter in 1958[35]. In his seminal work, he introduced a $\mathcal{P},\mathcal{T}$-odd perturbation term corresponding to a permanent eEDM into the one-electron Dirac equation in a Lorentz-covariant formulation. This term is analogous to the so-called "Pauli moment" interaction term (representing a QED interaction of the lowest order, for non-relativistic energies, between the electromagnetic field and the Pauli anomalous electric and magnetic dipole moments of the electron), but pre-multiplied by the pseudoscalar Dirac operator γ^5 (see pp. 47–51 of Ref. 36).

In atoms or molecules with at least one electron whose spin is unpaired, the effects arising from these $\mathcal{P},\mathcal{T}$-violating interactions produce atomic or molecular (permanent) $\mathcal{P},\mathcal{T}$-violating electric dipole moments that may be significantly larger than that of a free electron. In the past, it has been shown that the $\mathcal{P},\mathcal{T}$-violating EDM of these many-electron systems is mainly influenced by the electrostatic interactions between the eEDM of the unpaired electron and the internal electric fields[37]. Therefore, when calculating the molecular enhancement parameter W_{d} (see Eq. (1)) it is possible to ignore effects such as the interactions between the eEDM and the magnetic fields, and also the electron-electron Breit interactions.

When neglecting both, the interactions of the eEDMs with internal and external magnetic fields and the Breit interactions, the mean value of the Salpeter Hamiltonian can be equated to the expectation value of two different operators. One of these two effective Hamiltonians is the sum of only one-electron operators, while the other one also contains two-body operators. These two-electron contributions, however, are considerably smaller than the one-electron ones in that particular effective Hamiltonian, and as such they can usually be safely neglected[8,37].

Therefore, by employing any of these two effective Hamiltonians –denoted henceforth as scheme 1 (S1) and scheme 2 (S2)– to make theoretical predictions, one avoids having to treat the two-electron interactions of the Salpeter Hamiltonian, which are not negligible. The first of these effective Hamiltonians (i.e., within S1) has the form

$$\hat{H}^{\text{eEDM}}_{\text{eff-1}} = -d_{\text{e}} \sum_i (\boldsymbol{\beta}_i - \mathbb{1}_{4\times4}) \boldsymbol{\Sigma}_i \cdot \boldsymbol{E}(\boldsymbol{r}_i), \tag{8}$$

where the operator vectors $\boldsymbol{\Sigma}_i$ are related to the Pauli spin matrices by the expression

$$\boldsymbol{\Sigma} = \begin{bmatrix} \boldsymbol{\sigma} & \boldsymbol{\emptyset}_{2\times2} \\ \boldsymbol{\emptyset}_{2\times2} & \boldsymbol{\sigma} \end{bmatrix}, \tag{9}$$

and $\boldsymbol{E}(\boldsymbol{r}_i)$ is the total electrostatic electric field at the position of electron i, given by

$$\boldsymbol{E}(\boldsymbol{r}_i) = -\boldsymbol{\nabla}_i \left[\sum_K \Phi_K(\boldsymbol{r}_i) + \sum_{j\neq i} \Phi_j(\boldsymbol{r}_i) + \Phi^{\text{ext}}(\boldsymbol{r}_i) \right]. \tag{10}$$

Here, $\Phi^{\text{ext}}(\boldsymbol{r}_i)$ is the electrostatic potential produced by the external electric field at the position of electron i, whereas $\Phi_K(\boldsymbol{r}_i)$ and $\Phi_j(\boldsymbol{r}_i)$ are the potentials given in Eqs. (3) and (4). The sums over K and j in the first and second terms of Eq. (10) run over all the nuclei and all the electrons of the molecule, respectively.

In what follows, we neglect in Eq. (8) the effects arising from both external electric fields and the electric field produced by the electrons (i.e., the two-electron terms in $\hat{H}^{\text{eEDM}}_{\text{eff-1}}$), as their contributions to the molecular enhancement factors have been shown to be only on the order of one percent for heavy-element containing systems[8,17,37]. In this way, the effective Hamiltonian of S1 can be expressed as

$$\hat{H}^{\text{eEDM}}_{\text{eff-1}} \approx -d_{\text{e}} \sum_{i,K} (\boldsymbol{\beta}_i - \mathbb{1}_{4\times4}) \boldsymbol{\Sigma}_i \cdot \left[-\boldsymbol{\nabla}_i \Phi_K(\boldsymbol{r}_i) \right], \tag{11}$$

and if the nuclear charges are modeled using point-type density distributions (PN), then this effective Hamiltonian is given by the operator

$$\hat{H}^{\text{eEDM}}_{\text{eff-1 (PN)}} \approx -d_{\text{e}} \sum_{i,K} \frac{Z_K e}{4\pi\varepsilon_0} (\boldsymbol{\beta}_i - \mathbb{1}_{4\times4}) \boldsymbol{\Sigma}_i \cdot \frac{\boldsymbol{r}_i - \boldsymbol{R}_K}{|\boldsymbol{r}_i - \boldsymbol{R}_K|^3}, \tag{12}$$

where its dependence on the atomic number of the nuclei in the system is explicit.

The second effective eEDM Hamiltonian, within S2, includes only implicitly the two-electron interactions contained in the Salpeter formulation and is given by[37,38]

$$\hat{H}^{\text{eEDM}}_{\text{eff-2}} = i\, d_{\text{e}} \frac{2c}{e\hbar} \sum_i \boldsymbol{\beta}_i \boldsymbol{\gamma}^5_i \hat{p}^2_i, \tag{13}$$

where $\hat{p}^2 = -\hbar^2\, \hat{\nabla}^2$ and $\boldsymbol{\gamma}^5$ is the well-known Dirac matrix of dimension 4×4, defined as $\boldsymbol{\gamma}^5 = i\,\boldsymbol{\gamma}^0\boldsymbol{\gamma}^1\boldsymbol{\gamma}^2\boldsymbol{\gamma}^3$, with $\boldsymbol{\gamma}^0 = \boldsymbol{\beta}$ and $\boldsymbol{\gamma} = \boldsymbol{\beta}\boldsymbol{\alpha} = \boldsymbol{\gamma}^1\,\hat{\mathbf{i}} + \boldsymbol{\gamma}^2\,\hat{\mathbf{j}} + \boldsymbol{\gamma}^3\,\hat{\mathbf{k}}$. In terms of the $\boldsymbol{\sigma}_{x,y,z}$ Pauli spin matrices, $\boldsymbol{\gamma}^0 = \boldsymbol{\sigma}_z \otimes \mathbb{1}_{2\times2}$, $\boldsymbol{\gamma}^{1,2,3} = i\,\boldsymbol{\sigma}_y \otimes \boldsymbol{\sigma}_{x,y,z}$, and then $\boldsymbol{\gamma}^5 = \boldsymbol{\sigma}_x \otimes \mathbb{1}_{2\times2}$, where $\otimes$ implies a Kronecker product. Therefore, in the Dirac standard representation,

$$\boldsymbol{\gamma}^5 = \begin{bmatrix} \boldsymbol{\emptyset}_{2\times2} & \mathbb{1}_{2\times2} \\ \mathbb{1}_{2\times2} & \boldsymbol{\emptyset}_{2\times2} \end{bmatrix}. \tag{14}$$

Unlike the effective Hamiltonian $\hat{H}^{\text{eEDM}}_{\text{eff-1}}$ of Eq. (11), which explicitly depends on the nuclear charge density distributions $\rho_K(\mathbf{r})$, the Hamiltonian $\hat{H}^{\text{eEDM}}_{\text{eff-2}}$ given in Eq. (13) does not have a functional dependence on effects due to finite nuclear sizes. However, when perturbation theory is applied to calculate the molecular enhancement factor W_{d} using S2, these effects are implicitly accounted for through their explicit inclusion in the unperturbed Hamiltonian of the system, $\hat{H}^{(0)}$.

Furthermore, S2 only contains one-electron operators within an approximation in which both the magnetic interactions and the electron-electron Breit interactions are neglected, reducing the computational complexity. However, a drawback of this effective Hamiltonian is in the fact that the non-relativistic limit of its mean value is not zero, while that of the Salpeter Hamiltonian vanishes[39]. Furthermore, S2 does not allow analysis of the separate nuclear contributions to the calculated W_{d} parameters. Within S1, on the other hand, the non-relativistic limit of W_{d} is zero. While S1 includes two-electron contributions (see Eq. (8)), these are much smaller than the corresponding one-electron counterparts[17,37] and can usually be neglected. Therefore, S1 allows us to study the effective contributions to W_{d} arising from each nucleus of the system, keeping the correct non-relativistic behavior, and using only one-electron operators.

The interactions of the eEDMs with the internal electric fields can be taken as a perturbation on the DC Hamiltonian $\hat{H}^{(0)}$ of Eq. (2) and, in such case, the total (perturbed) electronic Hamiltonian is written as

$$\hat{H}^{\text{d}} = \hat{H}^{(0)} + \lambda\, \hat{H}^{\text{eEDM}}, \tag{15}$$

where λ is the dimensionless strength of the perturbation, and $\hat{H}^{\text{eEDM}}$ can be replaced either by $\hat{H}^{\text{eEDM}}_{\text{eff-1}}$ or $\hat{H}^{\text{eEDM}}_{\text{eff-2}}$.

The corrections to the molecular electronic energy arising from the perturbed Hamiltonian can be obtained by using Rayleigh–Schrödinger perturbation theory. A Taylor series expansion of the ground-state energy solution of Eq. (15), $E^{\text{d}}_\Omega(\lambda)$, can be written around $\lambda = 0$ as

$$E^{\text{d}}_\Omega(\lambda) = E^{(0)}_\Omega + \lambda\, E^{\text{d}(1)}_\Omega\Big|_{\lambda=0} + \frac{\lambda^2}{2}\, E^{\text{d}(2)}_\Omega\Big|_{\lambda=0} + \mathcal{O}(\lambda^3), \tag{16}$$

where the subindices Ω indicate that the ground-state solutions $|0\rangle$ of the unperturbed Hamiltonian $\hat{H}^{(0)}$ in a given fixed molecular frame and spin state fulfill the condition $\langle 0|\hat{\Omega}|0\rangle = \Omega$. For YbCu, YbAg, and YbAu, it can be seen that $|\Omega| = 1/2$[29]. Furthermore, the energy $E^{(0)}_\Omega = \langle 0|\hat{H}^{(0)}|0\rangle$ is the eigenvalue of the unperturbed Hamiltonian $\hat{H}^{(0)}$ in the same molecular frame. When

only the leading-order corrections are retained, and taking into account the relation between the effective spin-rotation Hamiltonian and the eEDM enhancement factor W_d given in Eq. (1), it can be shown that this parameter is given as

$$W_\mathrm{d} = \frac{1}{\Omega\, d_\mathrm{e}} \left.\frac{dE^\mathrm{d}_\Omega}{d\lambda}\right|_{\lambda=0} = \frac{1}{\Omega\, d_\mathrm{e}} \left.\left(\frac{d}{d\lambda}\left\langle 0^\mathrm{d}\middle|\hat{H}^\mathrm{d}\middle|0^\mathrm{d}\right\rangle\right)\right|_{\lambda=0}, \tag{17}$$

where $\left|0^\mathrm{d}\right\rangle$ is the ground-state solution of the perturbed Hamiltonian $\hat{H}^\mathrm{d}$.

B. S-PS-ne enhancement factor W_s

A second source contributing to the $\mathcal{P},\mathcal{T}$-violating interactions involving the electric dipole moment of an open-shell polar molecule in a $^2\Sigma_{\frac{1}{2}}$ ground state are the $\mathcal{P},\mathcal{T}$-odd S-PS-ne neutral-current interactions. Assuming that in each nucleus K the proton and neutron density distributions are equal to each other and also equal to the normalized nuclear density distribution $\varrho_K(\boldsymbol{r})$, the effective Hamiltonian that accounts for the four-fermion semi-leptonic interactions in the electron-nucleon sector (in the limit of infinitely heavy nuclei) can be written in terms of the proton-electron and neutron-electron interaction constants k^p_s and k^n_s, respectively, as[9,15,32]

$$\hat{H}^\mathrm{S-PS-ne} = i\frac{G_\mathrm{F}}{\sqrt{2}} \sum_{i,K} \left(Z_K k^\mathrm{p}_\mathrm{s} + N_K k^\mathrm{n}_\mathrm{s}\right) \boldsymbol{\beta}\boldsymbol{\gamma}^5_i \varrho_K(\boldsymbol{r}_i), \tag{18}$$

where N_K is the number of neutrons in nucleus K, G_F is the Fermi coupling constant (whose most recent value is $G_\mathrm{F}/(\hbar c)^3 = 1.1663787 \times 10^{-5}$ GeV^{-2}, or equivalently $G_\mathrm{F} \simeq 2.222516 \times 10^{-14}\, E_\mathrm{h}\, a_0^3$[40]), and $\varrho_K(\boldsymbol{r}_i) = \rho_K(\boldsymbol{r}_i)/(Z_K e)$ is the normalized nuclear density distribution of nucleus K at the position of the i-th electron, satisfying $\int \varrho_K(\mathbf{r})\, d^3\mathbf{r} = 1$. Besides, E_h and a_0 are the Hartree energy and Bohr radius, respectively. By defining a factor $k_{\mathrm{s},K} = k^\mathrm{p}_\mathrm{s} + (N_K/Z_K)\, k^\mathrm{n}_\mathrm{s}$, we can rewrite Eq. (18) as

$$\begin{aligned}\hat{H}^\mathrm{S-PS-ne} &= \sum_K \hat{H}^\mathrm{S-PS-ne}_K \\ &= i\frac{G_\mathrm{F}}{\sqrt{2}} \sum_{i,K} Z_K k_{\mathrm{s},K}\, \boldsymbol{\beta}\boldsymbol{\gamma}^5_i \varrho_K(\boldsymbol{r}_i).\end{aligned} \tag{19}$$

Making a treatment analogous to the one applied to the eEDM Hamiltonian, it is easy to see that the S-PS-ne Hamiltonian can also be taken as a perturbation (with field strength λ) to the 4c DC Hamiltonian, so that

$$\hat{H}^\mathrm{s} = \hat{H}^{(0)} + \lambda\, \hat{H}^\mathrm{S-PS-ne}. \tag{20}$$

By expanding the solution energy around $\lambda = 0$, the enhancement factor W_s can be obtained as

$$W_\mathrm{s} = \frac{1}{\Omega} \sum_K \frac{1}{k_{\mathrm{s},K}} \left.\frac{dE^{\mathrm{s},K}_\Omega}{d\lambda}\right|_{\lambda=0}. \tag{21}$$

III. COMPUTATIONAL DETAILS

The calculations reported in this work were performed using the DIRAC-19.0 program package[41,42]. The bond lengths were optimized using the exact two-components (X2C) Hamiltonian[43], the single-reference CCSD method, and s-aug-v4z basis set[44–46]. The active space energy cut-offs for the virtual (unoccupied) and occupied orbitals were set to $\pm 20\, E_\mathrm{h}$, $\pm 10\, E_\mathrm{h}$ and $\pm 10\, E_\mathrm{h}$ for YbCu, YbAg, and YbAu, respectively. A smaller active space was used for the heavier molecules since computing their bond lengths is computationally more intensive. The optimized internuclear distances for YbCu, YbAg, and YbAu are 2.7543 Å, 2.8589 Å, and 2.6524 Å, respectively. The bond length increases from YbCu to YbAg, and then decreases from YbAg to YbAu due to relativistic effects. A non-relativistic treatment would show longer bonds for heavier systems[47]. The enhancement factors were computed for these calculated equilibrium internuclear distances.

The molecular enhancement factors W_d and W_s were calculated using the four-component DC Hamiltonian and the multi-reference Fock-space coupled-cluster method with single and double excitations (FSCC)[48]. A multi-reference method is required for these calculations due to the challenging character of the ytterbium-containing molecules[49,50]. This method has been employed previously to study the enhancement factors of the $\mathcal{P},\mathcal{T}$-violating interactions in YbOH[51] and $YbCH_3$[52]. Additionally, the FSCC implementation within the EXP-T program[53,54] was used to investigate the effects of including triple excitations.

The uncontracted Dyall's valence-only basis sets of double-ζ (v2z), triple-ζ (v3z), and quadruple-ζ (v4z) quality were employed[55,56]. In addition, the core-valence basis sets (cv$X$z, $X = 2,3,4$) were used to examine effects arising from the correlation of core electrons[57]. These particular basis sets add tight functions with large exponents to the vXz basis sets. Finally, the augmented basis sets (s-aug-vXz) were employed to investigate how accurately the outer regions of the systems were described. The s-aug-vXz basis sets add a single diffuse function to each symmetry block.

Nuclear electric charge densities were modeled using point-type or spherically symmetric Gaussian distributions. For a given nucleus K, the charge density distributions corresponding to a point-type nucleus (PN) and a Gaussian-type nucleus (GN) are, respectively,

$$\rho^\mathrm{PN}_K(\boldsymbol{r}) = Z_K e\, \delta(\boldsymbol{r} - \boldsymbol{R}_K) \tag{22}$$

and

$$\rho^\mathrm{GN}_K(\boldsymbol{r}) = Z_K e \left(\frac{\zeta_K}{\pi}\right)^{3/2} e^{-\zeta_K\, |\boldsymbol{r}-\mathbf{R}_K|^2}. \tag{23}$$

Here, $\delta(\boldsymbol{r})$ is the Dirac delta distribution and $\zeta_K = 3/(2\langle R^2_{\mathrm{nuc},K}\rangle)$, with $\sqrt{\langle R^2_{\mathrm{nuc},K}\rangle}$ being the root-mean-square radius of the nucleus K, which can be obtained

using the empirical relation $\sqrt{\langle R^2_{\mathrm{nuc},K}\rangle} = (0.836\,A_K^{1/3} + 0.570)\,\mathrm{fm}$, where A_K is the mass number of the isotope of interest[58]. The most abundant isotopes were considered, i.e., ^{174}Yb, ^{63}Cu, ^{107}Ag, and ^{197}Au.

For calculations of W_s, identical nuclear models (either PN or GN) were used in both the $\hat{H}^{(0)}$ and $\hat{H}^{\mathrm{S-PS-ne}}$ operators (see Eqs. (2) and (19)). Besides, when W_d was calculated using S1, the PN model was employed in both $\hat{H}^{(0)}$ and $\hat{H}^{\mathrm{eEDM}}_{\text{eff-1 (PN)}}$ (see Eqs. (2) and (12)). The GN models were not yet implemented in DIRAC within $\hat{H}^{\mathrm{eEDM}}_{\text{eff-1}}$. Finally, computations of W_d within S2 were performed using either PN or GN models in the unperturbed Hamiltonian $\hat{H}^{(0)}$.

The enhancement factors were calculated by employing the finite-field method. In particular, by combining Eqs. (16), (17) and (21) it can be seen that they can be obtained by applying the two-point finite-field method, where

$$W_\mathrm{d} \approx \frac{1}{\Omega\, d_\mathrm{e}} \left[\frac{E^\mathrm{d}_\Omega(\lambda) - E^\mathrm{d}_\Omega(-\lambda)}{2\lambda}\right], \tag{24}$$

and

$$W_\mathrm{s} \approx \frac{1}{\Omega} \sum_K \frac{1}{k_{\mathrm{s},K}} \left[\frac{E^{\mathrm{s},K}_\Omega(\lambda) - E^{\mathrm{s},K}_\Omega(-\lambda)}{2\lambda}\right]. \tag{25}$$

Since $\hat{H}^{\mathrm{eEDM}}_{\text{eff-1}}$, $\hat{H}^{\mathrm{eEDM}}_{\text{eff-2}}$, and $\hat{H}^{\mathrm{S-PS-ne}}$ are $\mathcal{T}$-odd operators, they cannot be included at the level of the SCF iterations using DIRAC code. However, the total energy of the perturbed systems can be obtained by transforming the integrals of these operators from the (Dirac–Coulomb Hartree–Fock) scalar atomic primitive basis to the molecular spinor basis. Even though the applied algorithm is not yet described in detail in the literature, Ref. 59 provides some valuable information about the used formalism.

A field strength $\lambda = 10^{-6}$ was set when studying both parameters W_d and W_s in YbCu and YbAg, whereas $\lambda = 10^{-7}$ was used for the calculations involving YbAu.

Atomic units (i.e., $e = 1$, $a_0 = 1$, $\hbar = 1$, and $4\pi\varepsilon_0 = 1$) were used in all the calculations. For W_d, the values obtained following Eq. (24) were converted to the units used throughout this work using a conversion factor equal to the atomic unit (a.u.) of the electric field $E_\mathrm{h}/(e\,a_0) = 1.243380059 \times 10^{24}\ \frac{h\,\mathrm{Hz}}{e\,\mathrm{cm}}$. To calculate W_s following Eq. (25), the energies $E^{\mathrm{s},K}_\Omega(\pm\lambda)/k_{\mathrm{s},K}$ were obtained in a.u. as mean values of the Hamiltonian

$$\hat{H}^{(0)} \pm \frac{\lambda}{k_{\mathrm{s},K}} \frac{\sqrt{2}\,E_\mathrm{h} a_0^3}{G_\mathrm{F}\,Z_K} \hat{H}^{\mathrm{S-PS-ne}}_K, \tag{26}$$

and then the factor $G_\mathrm{F}\,Z_K/(\sqrt{2}\,a_0^3) = Z_K\,0.103403426\,h\,\mathrm{kHz}$ was used to convert the values of $W_{\mathrm{s},K}$ from a.u. to $h\,\mathrm{kHz}$. All values of the fundamental constants were taken from Ref. 40.

TABLE I. Reference values of W_d (employing S2) and W_s for YbCu, YbAg and YbAu. These results were obtained on the FSCCSD/v3z level of theory, using Gaussian-type nuclear models, and freezing 2, 4, and 56 electrons, respectively.

Molecule	$W_\mathrm{d}\ \left[10^{24}\ \frac{h\,\mathrm{Hz}}{e\,\mathrm{cm}}\right]$	$W_\mathrm{s}\ [h\,\mathrm{kHz}]$
YbCu	13.122	–47.647
YbAg	11.869	–44.361
YbAu	1.326	6.979

IV. RESULTS AND DISCUSSION

To obtain accurate enhancement factors accompanied by well-defined uncertainties, multiple computational aspects will be addressed. For all the calculations discussed in this section, the 4c DC Hamiltonian was employed. First, the baseline results will be presented in Section IV A. Then, the effect of selecting two different nuclear charge density distribution models is examined for both factors in Section IV B. Furthermore, the two schemes employed for computing W_d will be compared in Section IV C. Next, the influence of the basis set will be determined in Section IV D. Thereafter, different computational approaches will be compared in Section IV E. Finally, the effect of the geometry of the system on W_d and W_s will be discussed in Section IV F.

This extensive investigation allows us to set uncertainties on the final values. The justification for the final results and their uncertainties will be given in Section IV G.

A. Baseline calculations

All the reference values for W_d and W_s were computed on the v3z/FSCCSD level, using the equilibrium bond lengths obtained in this work and Gaussian-type nuclear charge distribution models. The reference values for W_d have been obtained using S2 (see Eq. (13)). For YbCu and YbAg, a virtual space cut-off of $500\,E_\mathrm{h}$ was employed, and 2 and 4 electrons were frozen, respectively. For YbAu, the virtual space cut-off was set to $40\,E_\mathrm{h}$, and 56 electrons were frozen. The selection of these correlation parameters is justified in Table S1 of the Supplementary Material.

The calculated enhancement factors for the three systems are given in Table I. We can observe that both parameters are very similar for YbCu and YbAg, while much lower absolute values are obtained for YbAu. This finding will be elucidated in the following sections. Furthermore, multiple corrections to these baseline values will be determined. The final obtained values will be given in Section IV G.

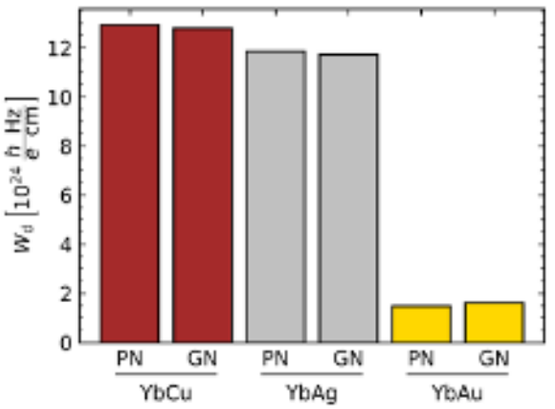

FIG. 1. Graphical representation of W_d (S2) for YbCu, YbAg, and YbAu using PN and GN models

. Results obtained on the FSCCSD/v2z level of theory, correlating all the electrons and using a virtual space cut-off of 3000 E_h.

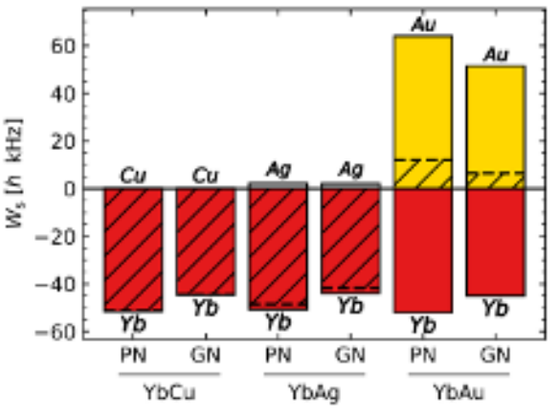

FIG. 2. Contributions to W_s for YbCu, YbAg, and YbAu, arising from each nucleus, using PN and GN models

. Results obtained on the FSCCSD/v2z level of theory, correlating all the electrons and using a virtual space cut-off of 3000 E_h. The hatched blocks correspond to the sum $W_{s,Yb} + W_{s,X}$ (X = Cu, Ag, Au).

B. Nuclear size effects

The effects arising from the use of two different nuclear models in the calculations of the molecular enhancement factors were investigated. For all three molecules, these effects were analyzed in both W_d and W_s. In this study, S2 has been employed to calculate W_d. All calculations were performed on the FSCCSD/v2z level of theory, correlating all electrons and using a virtual space cut-off of 3000 E_h for all three systems.

In Figure 1, the effects of using different nuclear charge density distribution models on W_d (S2) are shown (see also Table S3 in the Supplementary Material). For YbCu and YbAg, the results using GN are $\sim 1.1\%$ smaller than those obtained employing PN, while for YbAu the GN result is $\sim 9.2\%$ larger than the PN one. In particular, the nuclear size effects on YbCu and YbAg agree with those on YbF previously reported by Gaul and Berger in Ref. 17. Employing S1, they modeled the internal electric field of Eq. (11) using PN and GN models (using in both cases GN to model the unperturbed Hamiltonian) and found that these two results for YbF differ in $\sim 0.9\%$.

On the other hand, in Figure 2 the nuclear size effects on W_s. The contributions from each of the nuclei are shown, as well as the total values of W_s, represented by hatched blocks. The contributions associated with the nuclei of the coinage metals become increasingly important as their atomic number increases. Moreover, as expected, these contributions are of opposite sign to those of ytterbium because the gradients of the nuclear densities have opposite directions in the region between the two nuclei. For YbAu, the two contributions almost cancel each other out, leading to a very small total value of W_s (see Table S4 in the Supplementary Material).

In all three cases, the contribution of the ytterbium nucleus is reduced by $\sim 13\%$ when going from PN to GN, while for copper, silver, and gold the reduction is $\sim 0.16\%$, $\sim 3.5\%$, and $\sim 20\%$, respectively. Thus, the effect of using a finite nucleus model becomes more significant for the heavier elements, as can be expected. The total absolute W_s is also lower for the calculations performed using the GN model.

C. W_d: Comparison of schemes 1 and 2

It is well known that when the electric field produced only by the nuclei is taken into account in S1, the two schemes described in Section II A should yield similar results for W_d[37]. While the use of S2 is computationally less demanding, since it requires just a single calculation per system instead of the two that are required for each diatomic molecule, S1 allows us to examine the effective contributions arising from each nucleus. To study those individual contributions, we present (to the best of our knowledge) the first four-component results of W_d using the approximate effective Hamiltonian of Eq. (12), corresponding to the use of S1.

The molecular enhancement factors W_d were computed using both schemes (S1 and S2) on the FSCCSD/v2z level of theory, using PN model. Symmetric cut-offs of 500 E_h, 500 E_h, and 40 E_h were employed for YbCu, YbAg and YbAu (freezing 2, 4, and 56 electrons), respectively. It is worth mentioning that the differences between the values of W_d computed according to S1 and S2 (using GN for the unperturbed Hamiltonian and the internal electric field of the perturbation in S1) have been previously studied using two-component methods in a set of almost 30 diatomic molecules[17].

In Figure 3 we show the differences in W_d when computed with the two schemes for the three systems (see also Table S5 in the Supplementary Material). The values of W_d for YbCu and YbAg calculated using S1

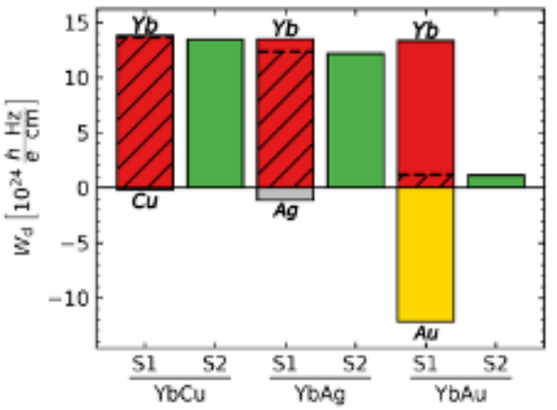

FIG. 3. Graphical representation of the behavior of W_d of YbCu, YbAg and YbAu computed using S1 and S2. For S1, the contributions from both nuclei are shown as well as their sums (hatched blocks). These results were obtained on the FSCCSD/v3z/PN level of theory, with a symmetric virtual space cut-off.

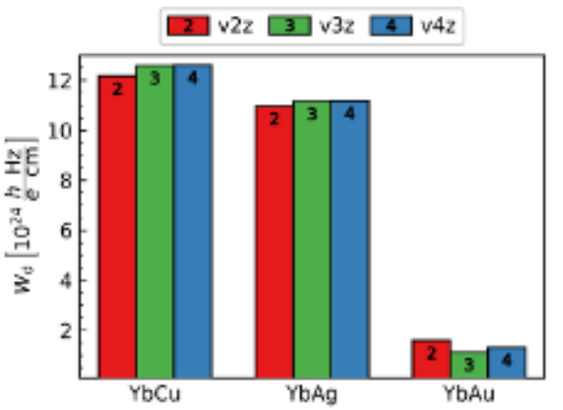

FIG. 4. The W_d (S2) enhancement factors of YbCu, YbAg, and YbAu, computed at the FSCCSD level of theory using GN models, and employing v2z, v3z, and v4z basis sets.

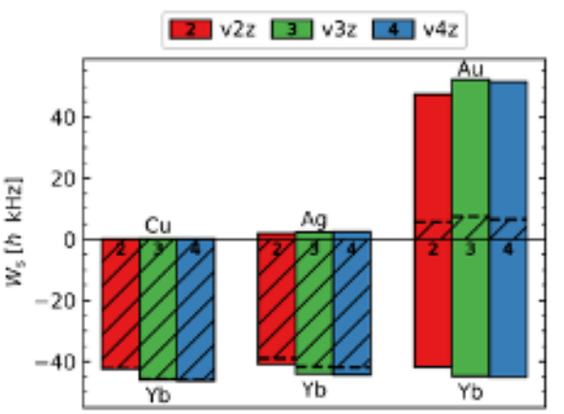

FIG. 5. The W_s enhancement factor of YbCu, YbAg and YbAu, for v2z, v3z and v4z basis sets, individual contributions from each nucleus. Computations were performed at the FSCCSD level of theory, using GN models . The hatched blocks correspond to the sum of the contributions from both elements.

are about 1.5% higher than those obtained using S2; this difference is 5% for YbAu. These differences may arise from contributions due to two-electron interactions, which are not taken into account in our implementation of S1 but are implicitly included in S2, but also from our use of finite basis sets, which could lead to different representation qualities of the different involved operators. These contributions are on the order of 1% for molecules containing one predominant heavy element (YbCu and YbAg), in agreement with previous predictions[8,17,37,60].

Using S1, it can be seen that the contributions to W_d from the Yb nucleus remain almost constant for all three systems. Moreover, the contributions from the coinage metals all have opposite signs to those coming from Yb, as is the case for the W_s factors. This is expected since the electric fields due to the two nuclei in the internuclear region have opposite directions, and according to Eqs. (11) and (12), this generates opposite contributions to this enhancement parameter. The decreasing total W_d factor from YbCu to YbAu is due to the increasing contribution from the second nucleus (opposite to that of the first).

D. Basis set effects

To observe how the size of the basis set influences the enhancement factors, W_d (S2) and W_s were computed with double-ζ, triple-ζ and quadruple-ζ quality basis sets. These calculations were done using GN models, FSCCSD method, and the (occupied and virtual) active space cut-offs were set to $\pm 20\,E_h$, $\pm 10\,E_h$ and $\pm 10\,E_h$, freezing 38, 64 and 82 electrons of YbCu, YbAg and YbAu, respectively.

The plot in Figure 4 shows the effect of increasing the basis set cardinality on W_d (see Table S6 in the Supplementary Material). Deviations of at most 3.5% are observed when this enhancement factor is calculated for YbCu and YbAg using v2z and v4z basis sets, whereas these differences reduce to less than 0.5% when v3z and v4z results are compared. While no apparent convergence can be observed for the total W_s values of YbAu, this convergence can be seen by looking at the individual contributions in Figure 5. A similar trend is expected for W_d.

Apart from adding contributing functions to all orbitals, it is also possible to add only tight or diffuse functions. Tight functions should increase the accuracy of the description of the core region of the system, while diffuse functions should improve the accuracy of the description of the valence region of the system. For these calculations, we used the cv$X$z basis sets that contain higher

angular momentum tight functions, and the s-aug-vXz basis sets that augment a diffuse function per symmetry to the vXz basis set. These computations were done using the same computational settings as the ones above.

The effects arising from increased accuracy in describing the core and valence regions of the systems are small for both enhancement factors. Adding tight functions has a negligible effect on all three systems for W_d (with the largest change of 0.4%) and W_s (with the largest change of 0.3%). On the other hand, adding diffuse functions reduces the parameter values slightly (with the largest changes of 2.9% and 1.9% for W_d and W_s, respectively). Furthermore, the enhancement factors of the YbAg system are more affected than those of YbCu. For YbAu, the addition of diffuse functions increases the calculated W_d and decreases the W_s. Still, the relative effects remain within 3% of the total value, as can be seen in Table S6 and Fig. S4 of the Supplementary Material.

For the final calculations, the v3z basis set was used for baseline results, and then corrections due to basis set quality and a better description of the core and valence regions were added. The incompleteness of the basis sets were also taken into account in the treatment of uncertainties.

E. Electron correlation effects

The method used so far throughout this work for calculations of the enhancement factors was 4c Dirac–Coulomb FSCC. Other approaches to calculate W_d (S2) and W_s have been analyzed, and the results are compared in Table II and Figures 6 and 7. These methods are DHF, Møller–Plesset up to second order (MP2), FSCCSD, and FSCCSDT. The calculations were performed employing the dyall.v2z basis set, GN models, and the active space cut-offs for the post-DHF computations were set to $\pm 2\,E_\mathrm{h}$, freezing 66, 84, and 116 electrons of YbCu, YbAg, and YbAu, respectively. This small active space and basis set were used because the inclusion of triple excitations (using the EXP-T program) is computationally expensive. The DHF results differ the most from the FSCC values, while the MP2 values are close to the FSCC results for YbCu and YbAg. On the other hand, going from MP2 to FSCC reduces the value of W_d for YbAu by a factor of two and reverses the sign of W_s.

Including the triple excitations in the FSCC calculations has only a minor effect on the enhancement factors of YbCu and YbAg, but increases the W_d and decreases the W_s of YbAu significantly, in line with enhanced sensitivity of this systems to the other computational parameters. It should be pointed out that due to the small size of the basis set, the contribution of the triple excitations should be considered as an order-of-magnitude estimate, rather than an accurate prediction. The differences between the FSCCSD and FSCCSDT methods will be used to estimate the uncertainty due to neglect of the higher excitations in Section IV G.

TABLE II. Enhancement factors W_d (S2) and W_s of YbCu, YbAg, and YbAu computed at the DHF, MP2, and two different FSCC levels of approach. Computations were performed using v2z basis set and GN models

	W_d $\left[10^{24}\ \frac{h\,\mathrm{Hz}}{e\,\mathrm{cm}}\right]$			W_s $[h\,\mathrm{kHz}]$		
Method	YbCu	YbAg	YbAu	YbCu	YbAg	YbAu
DHF	9.652	7.044	3.770	–33.081	–32.547	–22.275
MP2	11.174	9.188	2.314	–38.670	–37.696	–15.822
FSCCSD	11.323	10.415	1.072	–39.162	–36.897	7.385
FSCCSDT	11.310	10.555	1.567	–39.210	–37.406	5.268

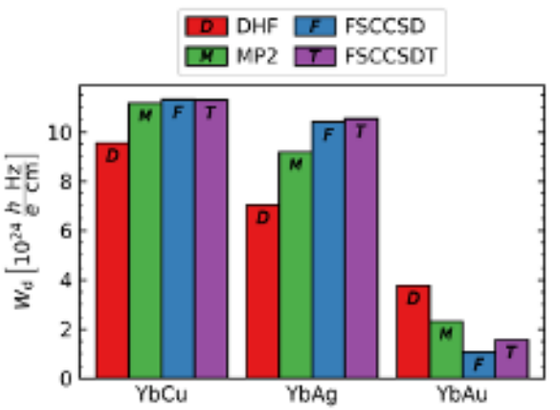

FIG. 6. The W_d (S2) enhancement factors of YbCu, YbAg, and YbAu computed at DHF, MP2, and FSCC levels of theory, using GN models. These computations were performed using the v2z basis set, and the active space cut-offs were set to $\pm 2\,E_\mathrm{h}$, freezing 66, 84, and 116 electrons of YbCu, YbAg, and YbAu, respectively.

F. Influence of molecular geometry

1. Bond length corrections

The equilibrium bond lengths used in all the calculations of the enhancement factors reported so far were obtained in Section III, as no experimental bond lengths are available for the systems considered in this work.

To investigate the influence of the bond lengths on the enhancement factors, these parameters were computed at the calculated equilibrium internuclear distances reported in Section III (using S2 for W_d), as well as at 0.05 Å and 0.1 Å larger and smaller internuclear distances. These computations were performed on the FSCCSD/v2z/GN level of theory, and the (occupied and virtual) active space cut-offs were set to $\pm 100\,E_\mathrm{h}$, $\pm 100\,E_\mathrm{h}$ and $\pm 95\,E_\mathrm{h}$, freezing 12, 20 and 28 electrons

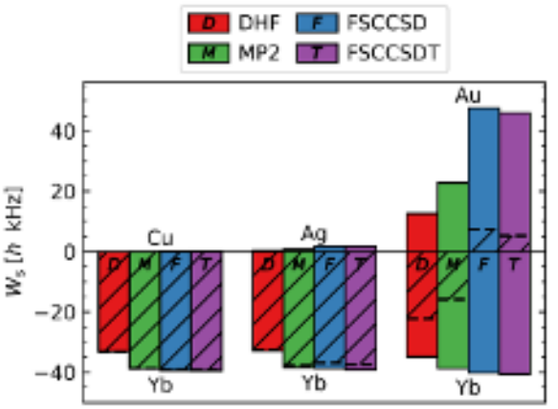

FIG. 7. The W_s enhancement factors of YbCu, YbAg, and YbAu computed at the DHF, MP2, and FSCC levels of theory, using GN models

. Results from each nucleus are given separately. The hatched blocks indicate the combined values. These computations were performed using the same basis set and active space cut-offs as in Figure 6.

TABLE III. Enhancement factors W_d (S2) and W_s of YbCu, YbAg, and YbAu, computed at different displacements (δ_R) with respect to the equilibrium bond lengths given in Section III. The computations were performed on the FSCCSD/v2z/GN level of theory.

	W_d [10^{24} $\frac{h\,\mathrm{Hz}}{e\,\mathrm{cm}}$]			W_s [h kHz]		
δ_R [Å]	YbCu	YbAg	YbAu	YbCu	YbAg	YbAu
–0.10	12.739	11.623	0.756	–44.186	–41.423	10.193
–0.05	12.630	11.556	1.211	–43.805	–41.138	8.106
0.00	12.512	11.477	1.619	–43.390	–40.813	6.219
0.05	12.383	11.385	1.981	–42.940	–40.445	4.532
0.10	12.242	11.280	2.297	–42.451	–40.036	3.041

of YbCu, YbAg and YbAu, respectively. The results are given in Table III. The absolute values of both enhancement factors of YbCu and YbAg decrease from the values at equilibrium bond lengths by less than 1.8% for the larger internuclear distance, and increase by 2.2% at most for the smaller bond length. For YbAu, the deviations are significantly larger, up to 64%.

Given the strong (and almost linear) dependence of the enhancement factors on the internuclear distances (see Table III), the bond lengths of YbCu, YbAg, and YbAu were re-optimized so that some effects that were not accounted for previously (especially perturbative triple excitations and a larger active space) can be considered. Since there are no experimental internuclear distances for our systems, we first analyzed six molecules for which there are available measurements with which our optimizations can be compared: YbX (X = F, Cl, Br)[61] and YAu (Y = Be, Mg, Ca)[62–64]. These optimizations were performed using the Molpro package[65,66], using a spin-free X2C Hamiltonian, ANO-RCC basis sets (with an effective cardinality larger than quintuple-ζ)[67–70], and treating electron correlation effects by using the single-reference CCSD(T) method, correlating all virtual orbitals and valence electronic orbitals (with a cut-off of –55 a.u.). The use of a scalar-relativistic framework is justified here as these molecules are studied in the $X\,^2\Sigma^+_{\frac{1}{2}}$ states. Our tests showed the differences due to the neglect of spin-orbit effects are below 0.01 Å, i.e. smaller than the effects of basis set size and electron correlation, which we were trying to address.

In all cases, these optimized bond lengths differ by less than 0.03 Å with respect to the available experimental values, with a mean absolute error of 0.012 Å (as can be seen in Table S11 of the Supplementary Material). Therefore, we can assume that the new internuclear distances obtained for YbCu, YbAg, and YbAu would have a similar error range. The same method was used to re-optimize the molecules of interest arriving at the final bond lengths of 2.7229 Å, 2.8329 Å, and 2.6975 Å for YbCu, YbAg, and YbAu, respectively. By fitting the enhancement factors and internuclear distances given in Table III with a linear function, we have corrected the values of W_d and W_s considering the new optimized distances. The results of these corrections are shown in Section IV G.

2. Vibrational corrections

The anharmonicity observed in the potential energy curves for the ground electronic states of YbCu, YbAg, and YbAu implies that their effective equilibrium bond lengths are slightly shifted compared to the minimum of the potential energy curves. These slight differences in bond lengths result in small changes in the enhancement factors.

To compute the vibrational corrections to W_d and W_s, calculations of these enhancement factors and the potential energies were performed for different bond lengths. The results for W_s, split up into the contributions arising from each nucleus can be found in Figure 8 (and also in Table S8 of the Supplementary Material). These values are given as a function of the difference between the internuclear distances and the equilibrium bond length of the corresponding molecule. The resulting $W_{s,\mathrm{Yb}/X}$ values are shown as a percentage compared to the results found at the equilibrium bond lengths given in Section III. It can be seen that the coinage metal contributions are significantly more sensitive to the bond-length effects compared to the Yb contributions. This is also in agreement with the sensitivity of the respective atoms to the description of the electronic structure, as can be seen in Figure 7 (and also in Table S7 of the Supplementary Material).

The vibrational corrections were computed using the VIBCAL module available in DIRAC-19.0, using a fourth-order polynomial for the energy fitting, and em-

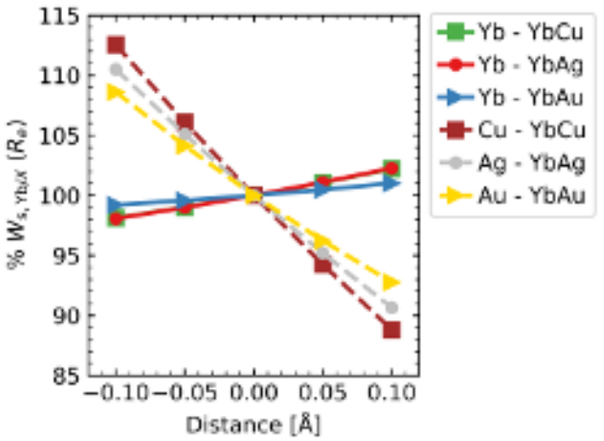

FIG. 8. The effect of the internuclear distance on the enhancement factor W_s of YbCu, YbAg and YbAu. These results were obtained on the FSCCSD/v2z/GN level of theory.

TABLE IV. Vibrational correction for both enhancement factors W_d (S2) and W_s. Results obtained on the FSCCSD/v2z/GN level of theory.

Molecule	$\Delta^{vib}W_d$ $\left[10^{24}\ \frac{h\,Hz}{e\,cm}\right]$	$\Delta^{vib}W_s$ $[h\,kHz]$
YbCu	–0.032	0.115
YbAg	–0.024	0.086
YbAu	0.013	–0.048

ploying enhancement factors calculated at the equilibrium bond length given in Section III, 0.01 Å, 0.05 Å and 0.1 Å larger and smaller internuclear distances. Scheme 2 was used to compute W_d. The calculations were performed on the FSCCSD/v2z/GN level of theory, and the active space cut-offs were set to $\pm100\,E_h$, $\pm100\,E_h$ and $\pm95\,E_h$ for YbCu, YbAg and YbAu, respectively. The vibrational corrections are listed in Table IV for both enhancement factors, and they alter the baseline values of the enhancement factor (obtained at R_{eq}) by $< 1\%$.

G. Final values and uncertainties

The baseline results given in Section IV A can now be corrected to obtain the final values of W_d and W_s, which can also be considered as recommended values based on this work. The contributions due to using a larger basis set, correlating all electrons, increasing the virtual space cut-offs, including triple excitations in the FSCC method, and taking into account bond length and vibrational corrections were added to the reference baseline values. Table V and Table S9 of the Supplementary Material present the values of these different contributions and the final values.

The basis set corrections were calculated as differences between FSCCSD calculations with active space cut-offs of $\pm20\,E_h$ for YbCu and $\pm10\,E_h$ for YbAg and YbAu, employing the dyall.v4z and dyall.v3z basis sets (see Table S6 of the Supplementary Material).

The effects arising from correlating all electrons were taken as the differences between freezing 2, 4, and 56 electrons for YbCu, YbAg, and YbAu respectively, and correlating all the electrons and simultaneously increasing the virtual cutoff to 6000 E_h at the FSCCSD/v2z level of theory. A detailed analysis of the effects of the active correlation space size is also available in Section I of the Supplementary Material.

The corrections due to the inclusion of higher excitations were taken as the differences between FSCCSDT and FSCCSD calculations, employing v2z basis sets and energy cut-offs of $\pm2\,E_h$. Finally, the effects arising from the corrected bond lengths were taken as described in Section IV F 1, and the vibrational effects were extracted from Table IV.

To provide conservative and reliable uncertainties for these enhancement factors, a treatment similar to that given in Refs. 71, 52, and 72 was employed. The uncertainties obtained from the discussed considerations are given in Table VI and Table S10 of the Supplementary Material, and analyzed individually in the following subsections.

1. Basis set

The uncertainties arising from the basis sets used in the calculations have three different sources: (i) the general quality of the basis sets (related to their cardinality), (ii) the number of extra tight functions, and (iii) the number of diffuse functions employed.

The overall quality of the basis sets affects the uncertainty of the final results because they cannot be considered fully converged at the v4z level. The baseline values are corrected by adding the differences between the v4z and v3z results, as described in Section IV D, and also adding the differences between the s-aug-v3z and v3z results, and between the cv3z and v3z values.

For both parameters, the uncertainties in basis set quality are seen to mainly arise from the differences between v4z and v3z results. These differences are taken as the uncertainties related to the basis set cardinality.

The uncertainties due to the possible insufficient amount of tight functions were taken into account as the differences between the cv3z and the v3z results. Finally, the differences between the s-aug-v3z and v3z values were taken as the uncertainties in the treatment of diffuse functions.

TABLE V. Final values of W_d (S2) and W_s for YbCu, YbAg, and YbAu, using GN models. The various corrections to the baseline values are assumed to be independent of each other.

	W_d $\left[10^{24}\ \frac{h\,\mathrm{Hz}}{e\,\mathrm{cm}}\right]$			W_s $[h\,\mathrm{kHz}]$		
	YbCu	YbAg	YbAu	YbCu	YbAg	YbAu
Baseline values	13.122	11.869	1.326	–47.647	–44.361	6.979
Corrections						
Bond length	0.078	0.045	0.347	–0.272	–0.180	–1.613
Vibrational effects	–0.032	–0.024	0.013	0.115	0.086	–0.048
Basis set cardinality (v4z vs v3z)	0.020	0.035	0.192	–0.269	–0.239	–0.983
Extra diffuse functions (s-aug-v3z vs v3z)	–0.001	–0.005	–0.033	0.002	0.012	0.143
Extra tight functions (cv3z vs v3z)	0.000	0.001	0.005	0.000	–0.006	–0.024
Active space[a]	0.149	0.135	0.016	–0.517	–0.483	1.478
Higher excitations[b]	–0.013	0.139	0.495	–0.047	–0.509	–2.117
Final values	13.323	12.195	2.361	–48.635	–45.680	3.815

[a] All-electron/+6000 E_h vs ±500 E_h (except for YbAu, where ±40 E_h was the reference), with v2z basis set.
[b] FSCCSDT vs FSCCSD calculations, with an active space cut-off of ±2 E_h and v2z basis set.

TABLE VI. The various sources of uncertainty for W_d (using S2) and W_s of YbCu, YbAg and YbAu. The uncertainties are assumed to be independent of each other.

	$\lvert\delta W_\mathrm{d}\rvert$ $\left[10^{24}\ \frac{h\,\mathrm{Hz}}{e\,\mathrm{cm}}\right]$			$\lvert\delta W_\mathrm{s}\rvert$ $[h\,\mathrm{kHz}]$		
Uncertainty source	YbCu	YbAg	YbAu	YbCu	YbAg	YbAu
Bond length[a]	0.129	0.092	0.362	0.451	0.368	1.686
Basis set						
Basis set cardinality (v4z – v3z)	0.020	0.035	0.192	0.269	0.239	0.983
Extra diffuse functions (s-aug-v3z – v3z)	0.001	0.005	0.033	0.002	0.012	0.143
Extra tight functions (cv3z – v3z)	0.000	0.001	0.005	0.000	0.006	0.024
Electron correlation						
Virtual space cut-off[b]	0.019	0.016	0.005	0.061	0.054	0.003
Higher excitations[c]	0.007	0.070	0.248	0.024	0.255	1.059
Sum of W_s approximation	–	–	–	0.059	0.308	1.313
Total uncertainty $\left(\sqrt{\sum_i(\delta_i W_{\mathrm{d/s}})^2}\right)$						
Absolute uncertainty	0.132	0.122	0.480	0.532	0.596	2.584
Relative uncertainty [%]	1.0	1.0	20.3	1.1	1.3	67.7

[a] Calculated as $|W_{\mathrm{d/s}}(R_\mathrm{eq} + 0.05\text{Å}) - W_{\mathrm{d/s}}(R_\mathrm{eq})|$. Values taken from Table III.
[b] Taken as 0.5 of the difference between FSCCSD calculations using all-electron/+6000 E_h and all-electron/+3000 E_h (employing v2z basis set).
[c] Taken as 0.5 of the difference between FSCCSDT and FSCCSD calculations, with an active space cut-off of ±2 E_h and v2z basis set.

2. Electron correlation

Electron correlation is affected by the chosen (occupied and virtual) active space cut-offs, along with the rank of excitations taken into account. To account for the frozen orbitals in the baseline calculations, the results provided in Table S1 and Figs. S1 and S2 of the Supplementary Material are used. The differences in enhancement factors between correlating all electrons and freezing 2, 4, and 56 electrons for YbCu, YbAg, and YbAu, respectively, were used to correct the baseline values, as shown in Table V; we thus do not assign uncertainties related to not correlating all the electrons.

The corrections for the limited virtual space cut-off that is used in the baseline calculations are taken as the differences between the obtained values at virtual space cut-offs of 6000 E_h and 500 E_h for YbCu and YbAg and between 6000 E_h and 40 E_h for YbAu. The v2z basis

set was used in these calculations, and the results are shown in Table V and also in Table S2 and Fig. S3 of the Supplementary Material.

To account for the effects of higher-lying virtual orbitals, half of the differences between the results obtained using virtual space cut-offs of 6000 E_h and 3000 E_h were taken as additional uncertainties (see Table VI).

The baseline values do not take into account triple excitations. The differences between the results obtained using FSCCSDT and FSCCSD methods, as described in Section IV E, were used to correct this omission. Since these results may not be fully converged yet, the effect of including triple excitations is used to estimate the uncertainty arising from not including quadruple and higher excitations, by multiplying by one-half the difference between the FSCCSDT and FSCCSD results.

3. Geometry

Inaccuracies in the calculated values of internuclear distances contribute to the enhancement factors' uncertainties. Based on our benchmark geometry calculations discussed in Section IV F 1, we conservatively set the uncertainty in the bond length to 0.05 Å and calculate the enhancement factors for internuclear distances ± 0.05 Å around R_eq (see Table III). The resulting differences were taken as the uncertainties associated with the molecular geometry.

4. Sum of atomic W_s approximation

Since the interaction constants $k_{\mathrm{s},K}$ in Eq. (19) are specific to each nucleus, calculating the total W_s value as a sum of the atomic contribution is only approximate and introduces an associated error. We analyze this error in detail in an upcoming publication[73]. Here, we provide the resulting uncertainties of 0.059 h kHz, 0.308 h kHz, and 1.313 h kHz for YbCu, YbAg, and YbAu, respectively. We note that the specific errors differ for each isotopologue. Therefore, here we use the isotopic average weighted by the natural abundances of all constituting elements.

5. Total uncertainty

To compute the total uncertainties for the reference values of the enhancement factors of YbCu, YbAg, and YbAu, the Euclidean norm of the individual uncertainties is taken. These total uncertainties are obtained on the assumption that the different contributions are largely independent since they concern high-order effects.

The relative uncertainties for W_s are similar to those found for W_d. For these systems, the enhancement factors are dominated by the uncertainty on the bond lengths, followed by the uncertainties due to missing higher CC excitations and, to a smaller degree, by the basis set incompleteness. The calculated values of W_s and W_d of YbCu and YbAg have uncertainties of about a single percent. A similar computational approach yielded uncertainties of $2\% - 7\%$ for the enhancement factors of BaF[71], $BaCH_3$, $YbCH_3$[52], and LaO, LaS, and LuO[72].

The results for YbAu have significantly higher relative uncertainties than those of the other two systems. Both enhancement factors of this system are relatively small due to a cancellation of large similar-sized contributions from the two constituent atoms, rendering them very sensitive to computational settings and leading to large relative uncertainty.

H. Comparison to other systems

The calculated enhancement factors are compared to those found for other ytterbium-containing molecules in Table VII. Additionally, some of the systems currently used in experiments aiming to restrict the lowest upper limit on the eEDM were added[11,12,74,75]. The W_d and W_s factors of YbCu and YbAg are of similar magnitude to those found for YbOH, $YbCH_3$, $YbOCH_3$ and YbF. Both enhancement factors of YbAu are significantly smaller than those found for any other ytterbium-containing system.

Since both the interactions of the eEDMs with electromagnetic fields and the S-PS-ne neutral-current interactions may contribute to an eventual experimental detection of $\mathcal{P},\mathcal{T}$-violating effects in molecules, these two types of interactions should be decoupled from each other. This can be done by performing measurements on systems with different enhancement factor ratios[17]. For the systems studied in this work, and some other molecules currently and previously under investigation, these ratios can be calculated from the values of enhancement factors reported in Table VII.

TABLE VII. Reference values of W_d and W_s for YbCu, YbAg, and YbAu compared to other Ytterbium-containing molecules and systems currently or previously investigated experimentally to determine the lowest upper limits on d_e and k_s.

System	Source	W_d $\left[10^{24}\ \frac{h\,\mathrm{Hz}}{e\,\mathrm{cm}}\right]$	W_s $[h\,\mathrm{kHz}]$
YbCu	This work	13.32(13)	–48.63(53)
YbAg	This work	12.19(12)	–45.68(60)
YbAu	This work	2.36(48)	3.81(258)
YbOH	Ref. 51	11.32(48)	
	Ref. 76	11.47	
	Ref. 77	8.54[b] ; 11.4[d]	–30.8[a] ; –41.2[c]
	Ref. 78	11.550	–41.318
	Ref. 79	11.3[b] ; 11.3[d]	–40.9[a] ; –40.9[c]
$YbCH_3$	Ref. 52	13.80(35)	–50.16(127)
$YbOCH_3$	Ref. 80	11.6	
YbF	Ref. 81	12.16	
	Ref. 82		–41.2
	Ref. 83	11.64	
	Ref. 84	11.17(89)	
	Ref. 85	11.23	–40.52(324)
	Ref. 60	10.0[a] ; 9.9[b] ; 11.6[c] ; 11.4[d]	
	Ref. 17	9.65[a] ; 9.55[b] ; 11.5[c] ; 11.4[d]	–34.6[a] ; –41.2[c]
	Ref. 79	11.2[b] ; 11.3[d]	–40.6[a] ; –40.9[c]
HfF^+	Ref. 86	5.49	20.0
	Ref. 79	5.66[b] ; 6.36[d]	20.7[a] ; 23.4[c]
ThO	Ref. 87	20.31	116
	Ref. 79	19.9[b] ; 24.1[d]	116[a] ; 141[c]
BaF	Ref. 88	3.64	
	Ref. 89	3.52	
	Ref. 90	2.5	
	Ref. 82		9.7
	Ref. 60	2.9[a] ; 2.9[b] ; 3.3[c] ; 3.3[d]	
	Ref. 17	2.91[a] ; 2.87[b] ; 3.33[c] ; 3.28[d]	7.58[a] ; 8.67[c]
	Ref. 91	3.15(30)	8.35(70)
	Ref. 71	3.13(12)	8.29(12)
	Ref. 79	3.02[b] ; 3.24[d]	7.98[a] ; 8.61[c]

[a] ZORA, complex generalized Kohn-Sham. W_d with S1.
[b] ZORA, complex generalized Kohn-Sham. W_d with S2.
[c] ZORA, complex generalized Hartree-Fock. W_d with S1.
[d] ZORA, complex generalized Hartree-Fock. W_d with S2.

V. CONCLUSION

Interpretation of experiments that search for $\mathcal{P},\mathcal{T}$-violating effects arising from both the interactions between eEDMs and electromagnetic fields and the S-PS-ne neutral-current interactions in molecules requires knowledge of the W_d and W_s enhancement factors, which can only be obtained through molecular electronic structure computations. In this work, these parameters were computed for the YbCu, YbAg, and YbAu systems, selected due to their possible experimental advantages. The enhancement factors W_d were calculated using two different schemes. This study confirms that, as indicated by previous predictions and studies[8,17,37,60], the two-body contributions to W_d represent only about 1% of its value in the case of systems with a predominance of one heavy element (YbCu and YbAg), but reach up to 5% for YbAu, formed from two heavy elements. Besides, a thorough uncertainty analysis was performed to assign a conservative error to the obtained results.

The final values were calculated using the FSCC method and the 4c DC Hamiltonian in conjunction with relativistic basis sets. The main contributing sources of uncertainty are due to the limited basis set size and the neglect of CC excitations beyond triples.

The obtained enhancement factors of YbCu and YbAg are of very similar size to other Yb-containing compounds investigated in the literature. In the case of YbAu, the cancellation of the contributions arising from the two nuclei in the system leads to vanishingly small total W_d and W_s values. For YbCu and YbAg, the results are also of similar size as for other systems currently investigated experimentally to search for signs of $\mathcal{P},\mathcal{T}$-violating effects. Compared to YbF and YbOH, the alternate method of producing and cooling these systems provides an alternative route for future experiments setting a new lowest upper limit on the eEDM.

SUPPLEMENTARY MATERIAL

In the Supplementary Material, we analyze the influence of the active space (in particular, of the energy of occupied and virtual correlated orbitals) on the calculation of W_d and W_s. We also present a set of tables where we report the values of these parameters using different nuclear models, different schemes corresponding to the use of the two effective Hamiltonians described in this work (for the case of W_d), and a few different basis sets. In addition, tables are provided showing the dependence of the molecular enhancement factors on the use of different methods to treat electron correlation, on vibrational effects, and also the contributions to W_d and W_s associated with each nucleus of the studied molecular systems.

ACKNOWLEDGMENTS

We would like to thank the University of Groningen's Center for Information Technology and the Dutch National Supercomputer for their support and for providing access to the Hábrók and Snellius high-performance computing clusters. This work made use of the Dutch national e-infrastructure with the support of the SURF Cooperative using grants no. EINF-5787, EINF-8014, and EINF-8532. We would like to express our gratitude to the anonymous referees who have made high-quality comments and suggestions, which have significantly improved this article. IAA thanks R. Berger and K. Gaul for inspiring discussions, and acknowledges partial support from FONCYT through grants PICT-2021-I-A-0933 and PICT-2020-SerieA-0052, and CON-

ICET through grant PIBAA-2022-0125CO. The work of IAA, AB, and SH was supported by the project *Probing Particle Physics with Polyatomic molecules* with project number OCENW.M.21.098 of the research programme M2 which is financed by the Dutch Research Council (NWO). The work of AB was also supported by the project *High Sector Fock space coupled cluster method: benchmark accuracy across the periodic table* with project number Vi.Vidi.192.088 of the research programme Vidi which is financed by the Dutch Research Council (NWO). The work of LFP and SH was supported by the project *Searching for missing antimatter with trapped molecules* with project number VI.C.212.016 of the research programme Vici which is financed by the Dutch Research Council (NWO). LFP acknowledges the support from the Slovak Research and Development Agency projects APVV-20-0098 and APVV-20-0127.

[1] M. K. Gaillard, P. D. Grannis, and F. J. Sciulli, "The standard model of particle physics," Rev. Mod. Phys. **71**, S96–S111 (1999).
[2] M. S. Safronova, D. Budker, D. DeMille, D. F. J. Kimball, A. Derevianko, and C. W. Clark, "Search for new physics with atoms and molecules," Rev. Mod. Phys. **90**, 3–40 (2018).
[3] T. S. Virdee, "Beyond the standard model of particle physics," Phil. Trans. R. Soc. A **374**, 1–15 (2016).
[4] Y. Gouttenoire, *Beyond the Standard Model Cocktail: A Modern and Comprehensive Review of the Major Open Puzzles in Theoretical Particle Physics and Cosmology with a Focus on Heavy Dark Matter*, 1st ed. (Springer Cham, 2023).
[5] J. Ginges and V. Flambaum, "Violations of fundamental symmetries in atoms and tests of unification theories of elementary particles," Phys. Rep. **397**, 63–154 (2004).
[6] P. Sandars, "Enhancement factor for the electric dipole moment of the valence electron in an alkali atom," Phys. Lett. **22**, 290–291 (1966).
[7] Y. Yamaguchi and N. Yamanaka, "Large Long-Distance Contributions to the Electric Dipole Moments of Charged Leptons in the Standard Model," Phys. Rev. Lett. **125**, 241802 (2020).
[8] P. Sandars, "The electric dipole moment of an atom," Phys. Lett. **14**, 194–196 (1965).
[9] M. G. Kozlov, "Semiempirical Calculations of P- and P, T-odd Effects in Diatomic Molecules-Radicals," Zh. Eksp. Teor. Fiz. **89**, 1933–1940 (1985), [Sov. Phys. JETP **62**, 1114 (1985), English translation by A. K. Agyei].
[10] O. P. Sushkov and V. V. Flambaum, "Parity breaking effects in diatomic molecules," Zh. Eksp. Teor. Fiz. **75**, 1208–1213 (1978), [Sov. Phys. JETP **48**, 608 (1978), English translation by W. H. Furry].
[11] T. S. Roussy, L. Caldwell, T. Wright, W. B. Cairncross, Y. Shagam, K. B. Ng, N. Schlossberger, S. Y. Park, A. Wang, J. Ye, *et al.*, "An improved bound on the electron's electric dipole moment," Science **381**, 46–50 (2023).
[12] ACME Collaboration, "Improved limit on the electric dipole moment of the electron," Nature **562**, 355–360 (2018).
[13] B. M. Schwarzschild, "Surprising upper limit on the electron's electric dipole moment," Phys. Today **67**, 15–17 (2014).
[14] Y.-Z. Li, M. J. Ramsey-Musolf, and J.-H. Yu, "Does the Electron EDM Preclude Electroweak Baryogenesis?" arXiv (Cornell University) , 1–6 (2024).
[15] V. G. Gorshkov, L. N. Labzovski, and A. N. Moskalev, "Effects of nonconservation of spatial and temporal parities in spectra of diatomic molecules," Zh. Eksp. Teor. Fiz. **76**, 414–421 (1979), [Sov. Phys. JETP **49**, 209 (1979), English translation by A. Tybulewicz].
[16] E. D. Commins, J. D. Jackson, and D. P. DeMille, "The electric dipole moment of the electron: An intuitive explanation for the evasion of Schiff's theorem," Am. J. Phys. **75**, 532–536 (2007).
[17] K. Gaul, S. Marquardt, T. Isaev, and R. Berger, "Systematic study of relativistic and chemical enhancements of $\mathcal{P}$, $\mathcal{T}$-odd effects in polar diatomic radicals," Phys. Rev. A **99**, 032509 (2019).
[18] L. D. Carr, D. DeMille, R. V. Krems, and J. Ye, "Cold and ultracold molecules: science, technology and applications," New J. Phys. **11**, 055049 (2009).
[19] L. R. Liu, J. T. Zhang, Y. Yu, N. R. Hutzler, Y. Liu, T. Rosenband, and K.-K. Ni, "Ultracold Molecular Assembly," (2017), arXiv:1701.03121 [physics.atom-ph].
[20] L. R. Liu, J. D. Hood, Y. Yu, J. T. Zhang, K. Wang, Y.-W. Lin, T. Rosenband, and K.-K. Ni, "Molecular assembly of ground-state cooled single atoms," Phys. Rev. X **9**, 021039 (2019).
[21] M. Verma, A. M. Jayich, and A. C. Vutha, "Electron Electric Dipole Moment Searches Using Clock Transitions in Ultracold Molecules," Phys. Rev. Lett. **125**, 1–2 (2020).
[22] G. Uhlenberg, J. Dirscherl, and H. Walther, "Magneto-optical trapping of silver atoms," Phys. Rev. A **62**, 063404 (2000).
[23] K. Honda, Y. Takahashi, T. Kuwamoto, M. Fujimoto, K. Toyoda, K. Ishikawa, and T. Yabuzaki, "Magneto-optical trapping of Yb atoms and a limit on the branching ratio of the $^1P_1$ state," Phys. Rev. A **59**, R934–R937 (1999).
[24] V. A. Dzuba, S. O. Allehabi, V. V. Flambaum, J. Li, and S. Schiller, "Time keeping and searching for new physics using metastable states of Cu, Ag, and Au," Phys. Rev. A **103**, 022822 (2021).
[25] M. Śmiałkowski and M. Tomza, "Highly polar molecules consisting of a copper or silver atom interacting with an alkali-metal or alkaline-earth-metal atom," Phys. Rev. A **103**, 022802 (2021).
[26] T. Fleig and D. DeMille, "Theoretical aspects of radium-containing molecules amenable to assembly from laser-cooled atoms for new physics searches," New J. Phys. **23**, 113039 (2021).
[27] J. Kłos, H. Li, E. Tiesinga, and S. Kotochigova, "Prospects for assembling ultracold radioactive molecules from laser-cooled atoms," New J. Phys. **24**, 025005 (2022).
[28] A. Marc, M. Hubert, and T. Fleig, "Candidate molecules for next-generation searches of hadronic charge-parity violation," Phys. Rev. A **108**, 062815 (2023).
[29] M. Tomza, "Interaction potentials, electric moments, polarizabilities, and chemical reactions of YbCu, YbAg, and YbAu molecules," New J. Phys. **23**, 1–12 (2021).
[30] O. Sushkov, V. Flambaum, and I. Khriplovich, "Possibility of investigating P-and T-odd nuclear forces in atomic and molecular experiments," Zh. Eksp. Teor. Fiz. **87**, 1521–1540 (1984), [Sov. Phys. JETP **60**, 873 (1984), English translation by J. G. Adashko].
[31] V. Flambaum, "Spin hedgehog and collective magnetic quadrupole moments induced by parity and time invariance violating interaction," Phys. Lett. B **320**, 211–215 (1994).
[32] J. Engel, M. J. Ramsey-Musolf, and U. van Kolck, "Electric dipole moments of nucleons, nuclei, and atoms: The Standard Model and beyond," Prog. Part. Nucl. Phys. **71**, 21–74 (2013).
[33] T. Chupp and M. Ramsey-Musolf, "Electric dipole moments: A global analysis," Phys. Rev. C **91**, 7 (2015).
[34] M. G. Kozlov and L. N. Labzowsky, "Parity violation effects in diatomics," J. Phys. B **28**, 1933–1961 (1995).
[35] E. E. Salpeter, "Some atomic effects of an electronic electric dipole moment," Phys. Rev. **112**, 1642–1648 (1958).
[36] H. A. Bethe and E. E. Salpeter, *Quantum Mechanics of One- and Two-Electron Atoms* (Springer, Berlin, 1957).
[37] E. Lindroth, B. W. Lynn, and P. G. H. Sandars, "Order α^2 theory of the atomic electric dipole moment due to an electric dipole moment on the electron," J. Phys. B **22**, 559–576 (1989).
[38] A.-M. Mårtensson-Pendrill and P. Öster, "Calculations of Atomic Electric Dipole Moments," Phys. Scr. **36**, 444 (1987).
[39] L. I. Schiff, "Measurability of nuclear electric dipole moments," Phys. Rev. **132**, 2194–2200 (1963).
[40] Tiesinga, E. and Mohr, P. J. and Newell, D. B. and Taylor, B. N., "The 2018 CODATA Recommended Values of the Fundamental Physical Constants (Web Version 8.1)," http://physics.nist.gov/constants, database developed by J. Baker, M. Douma, and S. Kotochigova (National Institute of Standards and Technology, Gaithersburg, 2018).
[41] DIRAC, a relativistic ab initio electronic structure program, Release DIRAC19 (2019), written by A. S. P. Gomes, T. Saue, L. Visscher, H. J. Aa. Jensen, and R. Bast, with contributions from I. A. Aucar, V. Bakken, K. G. Dyall, S. Dubillard, U. Ekström, E. Eliav, T. Enevoldsen, E. Faßhauer, T. Fleig, O. Fos-

sgaard, L. Halbert, E. D. Hedegård, B. Helmich-Paris, T. Helgaker, J. Henriksson, M. Iliaš, Ch. R. Jacob, S. Knecht, S. Komorovský, O. Kullie, J. K. Lærdahl, C. V. Larsen, Y. S. Lee, H. S. Nataraj, M. K. Nayak, P. Norman, G. Olejniczak, J. Olsen, J. M. H. Olsen, Y. C. Park, J. K. Pedersen, M. Pernpointner, R. di Remigio, K. Ruud, P. Sałek, B. Schimmelpfennig, B. Senjean, A. Shee, J. Sikkema, A. J. Thorvaldsen, J. Thyssen, J. van Stralen, M. L. Vidal, S. Villaume, O. Visser, T. Winther, and S. Yamamoto (available at http://dx.doi.org/10.5281/zenodo.3572669, see also http://www.diracprogram.org).

[42] T. Saue, R. Bast, A. S. P. Gomes, H. J. A. Jensen, L. Visscher, I. A. Aucar, R. Di Remigio, K. G. Dyall, E. Eliav, E. Faßhauer, T. Fleig, L. Halbert, E. D. Hedegård, B. Helmich-Paris, M. Iliaš, C. R. Jacob, S. Knecht, J. K. Lærdahl, M. Lopez Vidal, M. K. Nayak, G. Olejniczak, J. M. H. Olsen, M. Pernpointner, B. Senjean, A. Shee, A. Sunaga, and J. N. P. van Stralen, "The DIRAC Code for Relativistic Molecular Calculations," J. Chem. Phys. **152**, 204104 (2020).

[43] M. Iliaš and T. Saue, "An infinite-order two-component relativistic Hamiltonian by a simple one-step transformation," J. Chem. Phys. **126**, 064102 (2007).

[44] K. G. Dyall, "Relativistic double-zeta, triple-zeta, and quadruple-zeta basis sets for the 5d elements Hf–Hg," Theor. Chem. Acc. **112**, 403–409 (2004).

[45] K. G. Dyall, "Relativistic double-zeta, triple-zeta, and quadruple-zeta basis sets for the 4d elements Y–Cd," Theor. Chem. Acc. **117**, 483–489 (2007).

[46] A. S. P. Gomes, K. G. Dyall, and L. Visscher, "Relativistic double-zeta, triple-zeta, and quadruple-zeta basis sets for the lanthanides La–Lu," Theor. Chem. Acc. **127**, 369–381 (2010).

[47] P. Pyykko, "Relativistic effects in structural chemistry," Chem. Rev. **88**, 563–594 (1988).

[48] L. Visscher, E. Eliav, and U. Kaldor, "Formulation and implementation of the relativistic Fock-space coupled cluster method for molecules," J. Chem. Phys. **115**, 9720–9726 (2001).

[49] M. Denis, Y. Hao, E. Eliav, N. R. Hutzler, M. K. Nayak, R. G. E. Timmermans, and A. Borschesvky, "Enhanced P,T-violating nuclear magnetic quadrupole moment effects in laser-coolable molecules," J. Chem. Phys. **152**, 084303 (2020).

[50] C. Zhang, C. Zhang, L. Cheng, T. C. Steimle, and M. R. Tarbutt, "Inner-shell excitation in the YbF molecule and its impact on laser cooling," J. Mol. Spectrosc. **386**, 111625 (2022).

[51] M. Denis, P. A. B. Haase, R. G. E. Timmermans, E. Eliav, N. R. Hutzler, and A. Borschevsky, "Enhancement factor for the electric dipole moment of the electron in the BaOH and YbOH molecules," Phys. Rev. A **99**, 1–8 (2019).

[52] Y. Chamorro, A. Borschevsky, E. Eliav, N. R. Hutzler, S. Hoekstra, and L. F. Pašteka, "Molecular enhancement factors for the $\mathcal{P},\mathcal{T}$-violating electric dipole moment of the electron in $BaCH_3$ and $YbCH_3$ symmetric top molecules," Phys. Rev. A **106**, 052811 (2022).

[53] A. V. Oleynichenko, A. Zaitsevskii, and E. Eliav, "EXP-T, An Extensible Code for Fock Space Relativistic Coupled Cluster Calculations," (2020).

[54] A. V. Oleynichenko, A. Zaitsevskii, and E. Eliav, "Towards High Performance Relativistic Electronic Structure Modelling: The EXP-T Program Package," Commun. Comput. Inf. Sci. **1331**, 375–386 (2020).

[55] K. Dyall and A. Severo, "Revised relativistic basis sets for the 5d elements Hf–Hg," Theor. Chem. Acc. **125**, 97–100 (2009).

[56] K. G. Dyall, P. Tecmer, and A. Sunaga, "Diffuse basis functions for relativistic s and d block gaussian basis sets," J. Chem. Theory Comput. **19**, 198–210 (2022).

[57] K. G. Dyall, "Relativistic double-zeta, triple-zeta, and quadruple-zeta basis sets for the 6d elements Rf–Cn," Theor. Chem. Acc. **129**, 603–613 (2011).

[58] L. Visscher and K. G. Dyall, "Dirac-Fock atomic electronic structure calculations using different nuclear charge distributions," At. Data Nucl. Data Tables **67**, 207–224 (1997).

[59] L. Visscher, "The Dirac equation in quantum chemistry: Strategies to overcome the current computational problems," J. Comp. Chem. **23**, 759–766 (2002).

[60] K. Gaul and R. Berger, "Zeroth order regular approximation approach to electric dipole moment interactions of the electron," J. Chem. Phys. **147**, 014109 (2017).

[61] C. S. Dickinson, J. A. Coxon, N. R. Walker, and M. C. L. Gerry, "Fourier transform microwave spectroscopy of the $^2\Sigma^+$ ground states of YbX (X=F, Cl, Br): Characterization of hyperfine effects and determination of the molecular geometries," J. Chem. Phys. **115**, 6979–6989 (2001).

[62] J. Schiltz, "Étude des spectres optiques des composés de l'or avec les alcalinoterreux," Annales de Physique **13**, 67–106 (1963).

[63] R. F. Barrow, W. J. M. Gissane, and D. N. Travis, "Rotational analysis of the A-X and B-X systems of AuBe and AuMg," Proc. R. soc. Lond. Ser. A **287**, 240–258 (1965).

[64] C. Coquant and H. R., "Rotational Analysis of Au-Ca and Au-Si Radicals for Near Infrared Bands," C. R. Acad. Sci. Paris **284**, 171 (1977).

[65] H.-J. Werner, P. J. Knowles, R. Lindh, F. R. Manby, M. Schütz, *et al.*, "Molpro, version 2009.1, a package of ab initio programs," (2009), see http://www.molpro.net.

[66] H.-J. Werner, P. J. Knowles, F. R. Manby, J. A. Black, K. Doll, A. Heßelmann, D. Kats, A. Köhn, T. Korona, D. A. Kreplin, Q. Ma, I. Miller, Thomas F., A. Mitrushchenkov, K. A. Peterson, I. Polyak, G. Rauhut, and M. Sibaev, "The Molpro quantum chemistry package," J. Chem. Phys. **152**, 144107 (2020).

[67] V. Veryazov, P.-O. Widmark, and B. O. Roos, "Relativistic atomic natural orbital type basis sets for the alkaline and alkaline-earth atoms applied to the ground-state potentials for the corresponding dimers," Theor. Chem. Acc. **111**, 345–351 (2004).

[68] B. O. Roos, R. Lindh, P.-Å. Malmqvist, V. Veryazov, and P.-O. Widmark, "Main Group Atoms and Dimers Studied with a New Relativistic ANO Basis Set," J. Phys. Chem. A **108**, 2851–2858 (2004).

[69] B. O. Roos, R. Lindh, P.-Å. Malmqvist, V. Veryazov, and P.-O. Widmark, "New Relativistic ANO Basis Sets for Transition Metal Atoms," J. Phys. Chem. A **109**, 6575–6579 (2005).

[70] B. O. Roos, R. Lindh, P.-Å. Malmqvist, V. Veryazov, P.-O. Widmark, and A. C. Borin, "New Relativistic Atomic Natural Orbital Basis Sets for Lanthanide Atoms with Applications to the Ce Diatom and LuF_3," J. Phys. Chem. A **112**, 11431–11435 (2008).

[71] P. A. B. Haase, D. J. Doeglas, A. Boeschoten, E. Eliav, M. Iliaš, P. Aggarwal, H. L. Bethlem, A. Borschevsky, K. Esajas, Y. Hao, S. Hoekstra, V. R. Marshall, T. B. Meijknecht, M. C. Mooij, K. Steinebach, R. G. E. Timmermans, A. P. Touwen, W. Ubachs, L. Willmann, and Y. Yin, "Systematic study and uncertainty evaluation of P,T-odd molecular enhancement factors in BaF," J. Chem. Phys. **155**, 9–12 (2021).

[72] Y. Chamorro, V. V. Flambaum, R. F. Garcia Ruiz, A. Borschevsky, and L. F. Pašteka, "Enhanced parity and time-reversal-symmetry violation in diatomic molecules: LaO, LaS, and LuO," Phys. Rev. A **110**, 042806 (2024).

[73] L. F. Pašteka, I. A. Aucar, S. Hoekstra, and R. Timmermans, "Error analysis of the $\mathcal{P},\mathcal{T}$-odd nucleon-electron interaction in diatomic molecules," (2024), in preparation.

[74] J. Lim, J. R. Almond, M. A. Trigatzis, J. A. Devlin, N. J. Fitch, B. E. Sauer, M. R. Tarbutt, and E. A. Hinds, "Laser Cooled YbF Molecules for Measuring the Electron's Electric Dipole Moment," Phys. Rev. Lett. **120**, 123201.

[75] NL-eEDM Collaboration, "Measuring the electric dipole moment of the electron in BaF," Eur. Phys. J. D **72**, 197 (2018).

[76] V. S. Prasannaa, N. Shitara, A. Sakurai, M. Abe, and B. P. Das, "Enhanced sensitivity of the electron electric dipole moment from YbOH: The role of theory," Phys. Rev. A **99**, 062502 (2019).

[77] K. Gaul and R. Berger, "Ab initio study of parity and time-reversal violation in laser-coolable triatomic molecules," Phys. Rev. A **101**, 012508 (2020).

[78] A. Zakharova, I. Kurchavov, and A. Petrov, "Rovibrational structure of the ytterbium monohydroxide molecule and the P,T-violation searches," J. Chem. Phys. **155**, 164301 (2021).

[79] K. Gaul and R. Berger, "Global analysis of $\mathcal{CP}$-violation in atoms, molecules and role of medium-heavy systems," J. High Energ. Phys. , 100 (2024).

[80] C. Zhang, X. Zheng, and L. Cheng, "Calculations of time-reversal-symmetry-violation sensitivity parameters based on analytic relativistic coupled-cluster gradient theory," Phys. Rev. A **104**, 012814 (2021).

[81] N. S. Mosyagin, M. G. Kozlov, and A. V. Titov, "Electric dipole moment of the electron in the YbF molecule," J. Phys. B: At. Mol. Opt. Phys. **31**, L763 (1998).
[82] M. K. Nayak, R. K. Chaudhuri, and B. P. Das, "Ab initio calculation of the electron-nucleus scalar-pseudoscalar interaction constant W_S in heavy polar molecules," Phys. Rev. A **75**, 2 (2007).
[83] M. K. Nayak and R. K. Chaudhuri, "Re-appraisal of the P,T-odd interaction constant W_d in YbF: Relativistic configuration interaction approach," Pramana **73**, 581–586 (2009).
[84] M. Abe, G. Gopakumar, M. Hada, B. P. Das, H. Tatewaki, and D. Mukherjee, "Application of relativistic coupled-cluster theory to the effective electric field in YbF," Phys. Rev. A **90**, 022501 (2014).
[85] A. Sunaga, M. Abe, M. Hada, and B. P. Das, "Relativistic coupled-cluster calculation of the electron-nucleus scalar-pseudoscalar interaction constant W_s in YbF," Phys. Rev. A **93**, 042507 (2016).
[86] T. Fleig, "$\mathcal{P},\mathcal{T}$-odd and magnetic hyperfine-interaction constants and excited-state lifetime for HfF^+," Phys. Rev. A **96**, 040502 (2017).
[87] L. V. Skripnikov, A. N. Petrov, and A. V. Titov, "Communication: Theoretical study of ThO for the electron electric dipole moment search," J. Chem. Phys. **139**, 221103 (2013).
[88] M. G. Kozlov, A. V. Titov, N. S. Mosyagin, and P. V. Souchko, "Enhancement of the electric dipole moment of the electron in the BaF molecule," Phys. Rev. A **56**, R3326–R3329 (1997).
[89] M. K. Nayak and R. K. Chaudhuri, "Ab initio calculation of P, T-odd interaction constant in BaF: a restricted active space configuration interaction approach," J. Phys. B: At. Mol. Opt. Phys. **39**, 1231 (2006).
[90] E. R. Meyer, J. L. Bohn, and M. P. Deskevich, "Candidate molecular ions for an electron electric dipole moment experiment," Phys. Rev. A **73**, 062108 (2006).
[91] K. Talukdar, M. K. Nayak, N. Vaval, and S. Pal, "Relativistic coupled-cluster study of BaF in search of $\boldsymbol{\mathcal{CP}}$ violation," J. Phys. B **53**, 135102 (2020).